Simulation of Ice Formation by the Unstructured Finite Volume Method

Kuntinee Maneeratana
Department of Mechanical Engineering, Faculty of Engineering, Chulalongkorn University, Bangkok 10330
Tel: 0-2218-6610, Fax: 0-2252-2889, E-mail: kuntinee.m@chula.ac.th

Abstract

This paper simulates the formation of block ice by the unstructured finite volume method. The mathematical model is based upon the explicit heat conduction equation with the fixed grid, latent heat source approach. The main contributions on the solidification models are the comparison of pseudo-implicit temporal scheme and the gradually changing conductivities at solid-fluid interface against the explicit scheme and the use of solid conductivity, respectively. The temperature profiles, rates of ice formation and transfer energy in a 1D problem with prescribed boundary temperature are first compared with exact solutions. The results show that the most suitable schemes are still the combination of explicit and solid conductivity schemes. Then, the convective boundary condition is considered. Finally, the case study is simulated under 3D situations.

1. Introduction

Block ice manufacturers for food industries in Thailand have consumed huge amount of electricity in the manufacturing process. The purpose of this work is to develop a cheap 3D numerical simulation program for ice formation, leading to energy saving and improvements on the plant efficiency and profitability.

During the solidification process, the liquid/solid front, which releases massive latent heat, continuously progresses through the body under consideration. For ice formation, the problem is characterised by the isothermal phase change with abrupt discontinuity of properties at the constant freezing temperature. Thus, the problem is highly non-linear and exact solutions of the mathematical models are extremely difficult to obtain, giving raise to the popularity of numerical simulations.

The numerical procedures for phase change problems are categorises as combinations of two main models, the grid consideration and the latent heat representation. The grid consideration may be further divided into front tracking and fixed grid approaches while the latent heat is represented by either the temperature-based or the enthalpy-based method.

By comparing combinations of these approaches for the finite volume (FV) simulation [1], the fixed grid and the modified fictitious heat schemes is chosen such that the latent heat increment is calculated from the fictitious temperature in the freezing region and then the temperature fields are adjusted. In this previous study [1], the structured FV method solves 1 and 2D rectangular-grid test cases with prescribed boundary temperature. As the time step and grid sizes are severely restricted by the need to maintain one-cell freezing depth, the explicit scheme is recommended in place of the fully implicit and Crank-Nicolson schemes due to its lesser computational effort. The interface conductivity approximations are found to have strong influences. Comparing between arithmetic, harmonic means and solid conductivity, the best solutions are obtained with the solid approximation, which slightly overestimates the conductivities as the freezing front progresses across the saturated cells.

This paper expands the previous study [1] with an eye for practical uses. By re-examining the recommended numerical schemes, the ice formation is simulated using the arbitrary-shaped grids in the unstructured manner as the rectangular control volumes can not depict the tapering shape of the ice mould. In addition, the convective boundary is added. First, 1D phase change test cases with exact solutions or experimental measurements are studied; then, a real 3D problem is simulated. Interested variables and parameters include the temperature profiles, the ice thickness, rate of ice formation, fraction of water/ice and transfer energy.

2. Mathematical Model

The law of conservation of the energy is employed as the governing equation. With the Fourier's law of heat conduction for isotropic materials, the Lagrangian model is:

$$\frac{\partial H}{\partial t} = \frac{\partial}{\partial x_i}\left(k \frac{\partial T}{\partial x_i}\right), \tag{1}$$

where H, t, T, k and x_i represent the enthalpy, time, temperature, thermal conductivity and coordinates. The enthalpy is calculated from:

$$H = \int_{T_{ref}}^{T} \rho c_S \, dT \qquad \text{if } T < T_F,$$
$$H = \int_{T_{ref}}^{T_F} \rho c_S \, dT + \rho L + \int_{T_F}^{T} \rho c_L \, dT \qquad \text{if } T \geq T_F, \tag{2}$$

where ρ is mass density, c is the specific heat, L is the latent heat per unit mass, T_{ref} is the reference temperature and T_F is the freezing temperature. The subscripts S and L indicate the solid and liquid properties, respectively.

The boundary conditions are symmetry plane (zero heat flux), prescribed temperature and surface convection. The Newton's law of cooling states that the heat flux q^b leaving the fluid into solid per unit area by:

$$q^b = h(T^a - T^b), \tag{3}$$

where h is the heat transfer coefficient, T^b is the temperature at the solid boundary and T^a is the ambient fluid temperature.

It is noted that this work neglects effects of the radiation as well as all modes of convection, e.g. thermal, solidification expansion and bulk convection [1]. Thus, the density of the ice is approximated to that of the water to ensure the conservation of mass due to the lack of mass convection across cell faces.

3. Finite Volume Method

The mathematical model is formulated and discretised by a cell-centred finite volume technique for unstructured grids [2]. The

advantages of this scheme include the direct representation of conservative laws and straightforward physical interpretation.

3.1 Spatial and Temporal Discretisation

The spatial domain is discretised into a finite number of control volumes or cells. A typical cell with volume V^P (Figure 1) is represented by the node *P* at the centre and bounded by *n* cell faces *f* with normal, outwards surfaces S_i^f, which are shared between *P* and adjacent cells Q^f. In addition, non-computational nodes at boundaries are introduced for the specification of boundary conditions. This study uses hexahedron cells with 8 vertices, 12 edges and (4, 4, 4, 4, 4, 4) degree sequence.

The time domain is divided into an arbitrary number of time steps of size δt. Variables at time *t* are indicated by the superscript 0 while those at time level $t + \delta t$ are not.

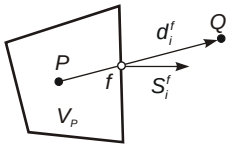

Figure 1 A typical unstructured control volume.

3.2 Mathematical Model Approximation

As the fictitious sensible heat is used, equations (1) and (2) are combined with the sensible heat term from (2) and converted into the integral form for any cell *P* as:

$$\int \rho c \frac{\partial T}{\partial t}\, dV^P = \sum_{f=1}^{n} \int k^f \frac{\partial T}{\partial x_i} dS_i^f \quad . \tag{4}$$

The second-order accurate spatial distribution of variables is assumed. The value of any quantity ϕ at a cell face *f* between *P* and Q^f is calculated by:

$$\phi^f = \frac{\phi^P + \phi^{Q^f}}{2} + \frac{(\partial\phi/\partial x_i)^P (r_i^f - r_i^P) + (\partial\phi/\partial x_i)^{Q^f} (r_i^f - r_i^{Q^f})}{2}, \tag{5}$$

where r_i is the position vector and the superscript denotes the location of the property. The gradient vector $(\partial\phi/\partial x_i)^P$ at cell *P* is calculated by ensuring a least square fit of ϕ through *P* and neighbouring nodes Q^f as:

$$\left(\sum_{f=1}^{nb} \frac{d_j^f d_i^f}{(d^f)^3} \right) \left(\frac{\partial\phi}{\partial x_i}\right)^P = \sum_{f=1}^{nb} \frac{(\phi^P - \phi^{Q^f}) d_j^f}{(d^f)^3} \quad , \tag{6}$$

where $d_i^f = r_i^{Q^f} - r_i^P$ is the distance vector between *P* and Q^f.

For the conductivity *k* at the cell faces, the uses of arithmetic mean k_a, harmonic mean k_h and solid value k_S are compared in [1]. The conductivity value at each cell faces is calculated from the average values of the adjacent control volumes, such that the 1D mean interface conductivity are:

$$k_a^f = k^P \left| r_i^f - r_i^{Q^f} \right| + k^{Q^f} \left[1 - \left| r_i^f - r_i^P \right| \right], \quad \frac{1}{k_h^f} = \frac{\left| r_i^f - r_i^P \right|}{k^P} + \frac{\left| r_i^f - r_i^{Q^f} \right|}{k^{Q^f}} . \tag{7}$$

The results show that the use of solid conductivity slightly overestimates the rate of heat transfer while the arithmetic mean underestimates the values. Meanwhile, the harmonic mean yield worst solutions due to the progression of solidification front across the cells.

In these cases, the numerical values of nodal conductivity k^P and k^{Q^f} are fixed as fully solid and liquid values and do not change with the increasing solidification of the connecting control volumes. Hence, if these nodal values are assumed to be linearly proportional to the water/ice ratio of the cells, the gradually increasing values of *k* are obtained.

The diffusion flux through the face *f* into an adjacent node Q^f is approximated using the orthogonal correction method as:

$$\int k^f \frac{\partial T}{\partial x_i} dS_i^f \approx k^f \left(\frac{T^Q - T^P}{d^f} + (\frac{\partial T}{\partial x_i})^f (\frac{S_i^f}{S^f} - \frac{d_i^f}{d^f}) \right) S^f \, . \tag{8}$$

For the convective boundary, the boundary temperature T^b is calculated by substituting Fourier's law and (3) into (8):

$$T^b (h + \frac{k^f}{d^f}) \approx k^f \left(\frac{T^P}{d^f} - (\frac{\partial T}{\partial X_i})^f (\frac{S_i^f}{S^f} - \frac{d_i^f}{d^f}) \right) + hT^a \, . \tag{9}$$

Then, the temperature at a boundary is incorporated into the cell equation by substituting T^Q by T^b in (8). Additionally, for convective boundary, the k^f at the boundary is assumed to be linearly proportional to the water/ice ratio of the cells.

In general, the temporal distribution of temperature is approximated by two-time level schemes such that:

$$\int_t^{t+\Delta t} \phi \, dt \approx \left[f\phi - (1-f)\phi^0 \right] \Delta t \, , \tag{10}$$

where *f* is a weighting factor with the value between 0 and 1. The first-order accurate explicit method uses temperature gradients of the previous time step *t* to calculate the unknown *T* at $t + \delta t$ such that $f = 0$. Although, the size of δt must be limited, for instance $\delta t < \rho c (\delta x)^2 / 2k$ for 1D problems, in order to guarantee numerical stability [3], the previous study [1] shows that the step size is far more severely restricted by the need to ensure that the freezing front composes of only one layer of control volumes.

By applying (5)-(10), equation (4) can be approximated as:

$$\frac{(\rho c V)^P}{\delta t} (T - T^0)^P \approx f \sum_{f=1}^{n} k^f \left[\frac{S^f}{d^f} (T^{Q^f} - T^P) + (\frac{\partial T}{\partial x_i})^f (S_i^f - \frac{S^f}{d^f} d_i^f) \right] + (1-f) \sum_{f=1}^{n} k^f \left[\frac{S^f}{d^f} (T^{Q^f} - T^P) + (\frac{\partial T}{\partial x_i})^f (S_i^f - \frac{S^f}{d^f} d_i^f) \right]^0 . \tag{11}$$

The equation (11) for each internal cell may be rearranged for the explicit scheme ($f = 0$) into:

$$\frac{(\rho c V)^P}{\delta t} (T - T^0)^P - \sum_{f=1}^{n} (k \frac{S}{d} T^Q)^{f,0} \approx \sum_{f=1}^{n} \left[k (\frac{\partial T}{\partial x_i}) (S_i - \frac{S}{d} d_i) \right]^{f,0} . \tag{12}$$

On the other hand, if the implicit scheme is used ($f = 1$) and it is assumed the small changes of temperatures during any time step, equation (4) can be approximated into a pseudo-implicit relationship as:

$$\frac{(\rho c V)^P}{\delta t} (T - T^0)^P \approx \sum_{f=1}^{n} \left[k \frac{S}{d} (T^{Q,0} - T^P) + k (\frac{\partial T^0}{\partial x_i}) (S_i - \frac{S}{d} d_i) \right]^f . \tag{13}$$

3.3 Solution Algorithm

By assembling equation (12) or (13) of all control volumes in the domain with appropriate initial and boundary conditions, the system of simultaneous algebraic equations $[A] \cdot [T] = [b]$ is formed with nodal temperature $[T]$ as unknowns.

The overview of the solution algorithm is shown in Figure 2. Prior to the first time interval, the accumulated latent heat of a

control volume P, Q^P , is initialised as zero. At the beginning of each time step, the phase status of each control volume is checked. If the nodal phase is liquid and the nodal temperature T^P drops lower than the freezing temperature T_F , the control volume becomes saturated and its node is tagged. Special attentions are given to the cell face conductivity, which depends on the status of the nodal phase.

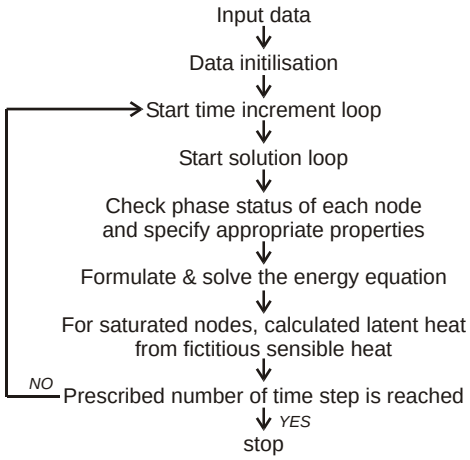

Figure 2 Explicit solution algorithm.

As the explicit schemes are used, the current temperature may be calculated directly from the past values. The nodal temperature is then reassigned to the freezing temperature and the latent heat increment, the energy used for phase change in the current time step, is calculated from the fictitious sensible heat such that $\Delta Q^P = \rho c(T_F - T^P)V^P$. The ΔQ^P is added to the accumulated Q^P for subsequent time steps until the accumulated latent heat equals the total latent heat $\rho L V^P$ available in the control volume. At this stage, the control volume becomes solid, the tag on the cell is removed and the latent heat increment is no longer calculated.

4. Results and Discussions

4.1 Case 1: 1D Prescribed Boundary Temperature

A 4-m-long domain of water with unit square cross section is initially at temperature $T_i = 10$°C . At time $t = 0$, the boundary at $x = 0$ is lowered to $T_c = -20$°C [1]. The freezing occurs at $T_F = 0$°C with $L = 338$ kJ/kg while other properties are shown in Table 1.

Table 1 Material properties of water and ice.

Properties	Water	Ice
k (W/m·K)	0.556	2.220
c (kJ/kg·K)	4.226	1.762
ρ (kg/m^3)	1000	1000*

*Approximate to the water value to ensure mass conservation [1]

Exact solutions for a semi-infinite slab are given in [4]. The dimensionless distance $s = x/2\sqrt{\alpha_S t}$ while the dimensionless distance of solid-fluid interface s_{SL} is determined from:

$$\frac{\exp(-s_{SL}^2)}{\text{erf}(s_{SL})} + \frac{T_F - T_i}{T_F - T_C}\frac{k_L}{k_S}\sqrt{\frac{\alpha_S}{\alpha_L}}\frac{\exp(-(\alpha_S/\alpha_L)s_{SL}^2)}{\text{erfc}(\sqrt{\alpha_S/\alpha_L}\,s_{SL})} = \frac{\sqrt{\pi}Ls_{SL}}{c_S(T_F - T_C)}, \quad (14)$$

where the thermal diffusivity $\alpha = k/\rho c$. The temperatures in solid and liquid regions are:

$$\frac{T_S(x,t) - T_c}{T_F - T_c} = \frac{\text{erf}(s)}{\text{erf}(s_{SL})}, \quad \frac{T_L(x,t) - T_i}{T_F - T_i} = \frac{\text{erfc}(\sqrt{\alpha_S/\alpha_L}\,s)}{\text{erfc}(\sqrt{\alpha_S/\alpha_L}\,s_{SL})}. \quad (15)$$

The combinations of explicit/pseudo-implicit temporal schemes and the $k_S/k_a/k_h$ interface conductivities are used. Domain is divided into uniform cells with prescribed boundary temperatures at both ends and insulation condition along the slab. It is found that the numerical stability and grid and time step independency with one-cell-deep freezing front are obtained with uniform cells of $\delta x = 0.01$ m and $\delta t = 10$ s .

As results from different schemes differ slightly, only solutions from the explicit scheme and k_S interface are displayed against exact solutions. Figure 3, showing the temperature profiles at various time instants, clearly illustrates that liquid cells cool down slowly; once a control volume is frozen, its temperature drops rapidly such that the temperature gradient in the ice is almost linear and the freezing of the next cell starts shortly after (Figure 4). That is, the rate of heat transfer is predominantly controlled by the position of the freezing front.

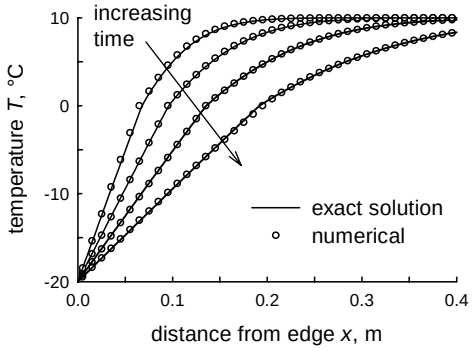

Figure 3 Case 1: Temperature at time 6, 12, 24 and 48 hr. The numerical solutions use the explicit/k_S schemes.

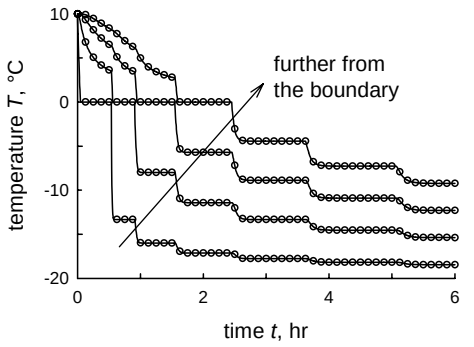

Figure 4 Case 1: Temperature history of 4 adjacent nodes to the boundary. The numerical solutions use the explicit/k_S schemes.

In addition, the low diffusivity, particularly in the liquid region, and low temperature gradient with isothermal solidification, the freezing front x_{SL} advances at ever slowing rate with the square root function of time as shown in Figure 5. In this graph, the numerical simulations show two different numerical data – the

location of saturated cells and the predicted ice thickness that is calculated from the location of saturated cells and the accumulated latent heat Q^P of the control volume. It is also shown that the graph of the total energy loss U (Figure 6), which is calculated from the enthalpy H, exhibits a similar shape such that the total power loss dU/dt , or the cooling load, drops rapidly during the first few hours.

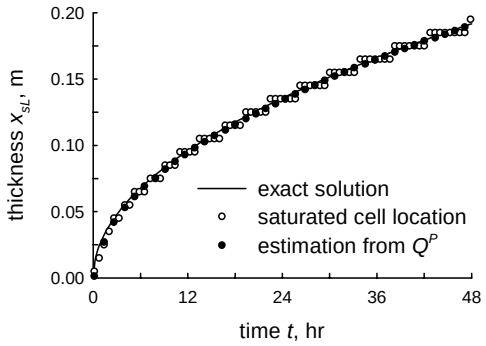

Figure 5 Case 1: Ice thickness. The numerical solutions use the explicit/k_S schemes.

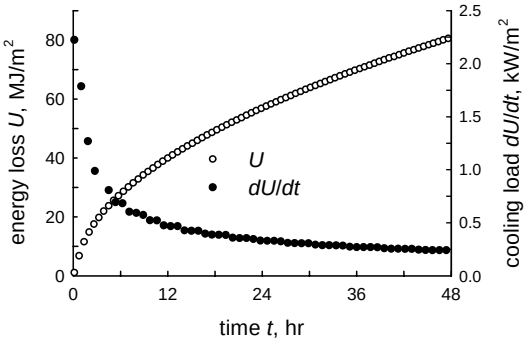

Figure 6 Case 1: Loss of internal energy and cooling loads of the system. The numerical solutions use the explicit/k_S schemes.

Unlike in which the temperature profile is given prominence, the control of ice manufacturing plants requires the information on percentages of solidified volumes, which can be indirectly represented by the ice thickness, and the amount of heat transfer out of the ice block [5]. Hence, both errors of the temperature $\varepsilon(T^P)$ and ice thickness $\varepsilon(x_{SL})$ are investigated.

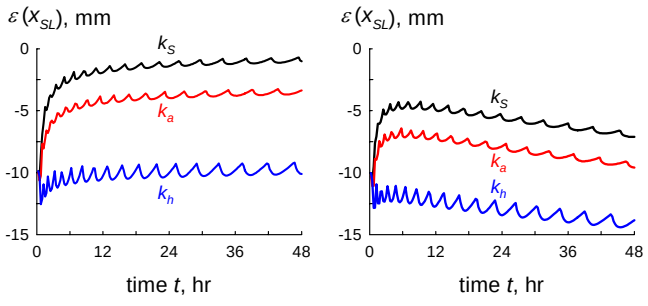

Figure 7 Case 1: Ice thickness errors.

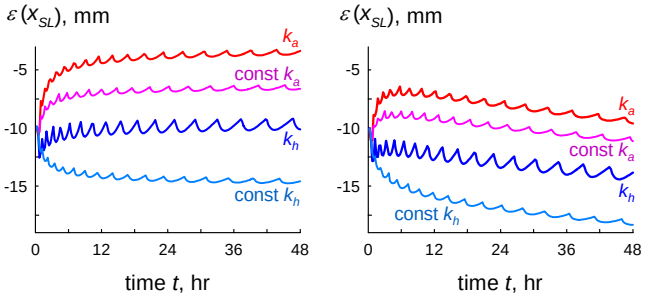

Figure 8 Case 1: Comparisons of ice thickness errors from simulations with constant and varying mean conductivities.

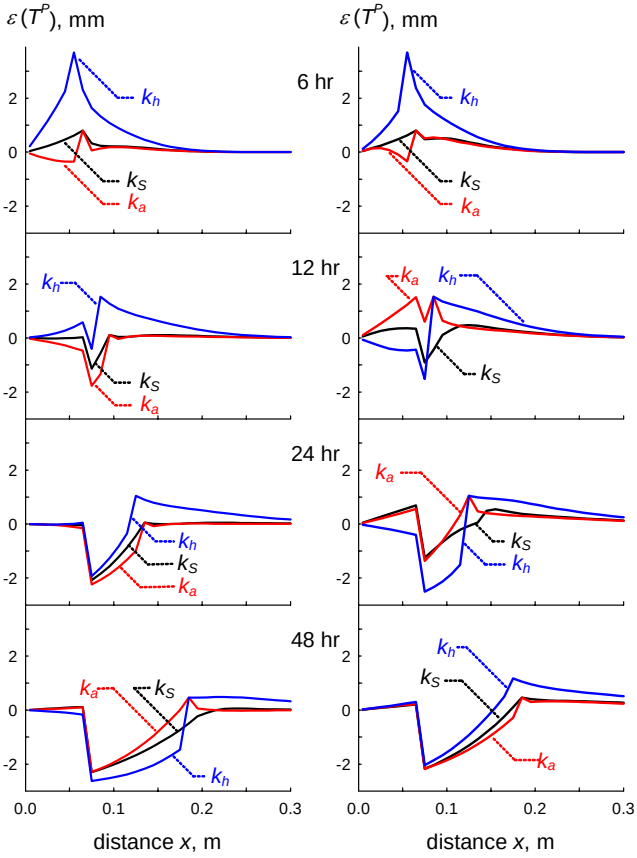

Figure 9 Case 1: Temperature errors at time 6, 12, 24 and 48 hr.

Figure 7 shows that all numerical schemes underestimate the rate of ice formation with high error values during the first few hours due to the high initial disturbance from the high rate of cooling load (Figure 6) and temperature gradient before the system are stabilised into two different characteristics – the explicit results converged closer to zero while the pseudo-implicit solutions fall further and further behind the exact values.

When different interface conductivities are compared, the k_S approximation yields best numerical results, followed by k_a and k_h. The slight overestimation of the k_S face conductivity at the short instants before the solidification front stays at the interface between two control volumes help compensating the underestimations of the temporal schemes. For the mean

conductivities k_a and k_h, the use of continuously changing values simulates the actual phenomenon more closely and helps increasing the accuracy when compared to the constant mean values in [1] as shown in Figure 8.

These findings concur with [1] that the implicit scheme underestimates the rate of ice formation more than the more explicit ones. The ripples common to all thickness error curves, corresponds to the solidification of one control volumes and suggests the localised disorder from the release of large amount of latent heat. It is noted that even though Figure 7a show the lessening of errors, the predicted errors becomes constant and never reaches nor exceeds the exact solutions such that around 800 hr, the errors oscillate between -0.5 – 0.2 mm.

When the temperature errors (Figure 9) are considered, it is found that during the first few hours, the errors are high, again, due to the strong initial system disturbances. Additionally, the location of maximum errors remains at the same local area due to the accumulation during the initial hours even as the region of high errors expands with increasing time, following the progression of water/ice front.

As the critical information for the plant management is the cooling load and the fraction of water/ice, the combination of explicit and solid conductivity schemes are recommending for practical problems due to their best accuracy and low computational efforts in the prediction of solidification front progression.

4.2 Case 2: 1D Convective Boundary

The problem is set up in comparison with another related experiment which measures ice thickness [6]. A very long domain of water is initially at freezing temperature of $T_i = 0°\text{C}$. At time $t = 0$, the ambient temperature is lowered to $T_a = -8°\text{C}$ with the coefficient $h = 1500\ \text{W/m}\cdot\text{K}$. It should be note that in the experiment there is an additional stainless 3.77-mm-thick steel wall in the experiment, resulting in the environment/wall boundary convection and the wall/ice interfaces instead of the environment/ice boundary condition. As steel is a much better conductor than ice, this assumption should not cause much error.

The modelling employs the same the domain, control volume size, time steps and material properties as in case 1. The numerical solutions use the explicit and k_S schemes. As the sensible temperature is used to check the phase status of the control volumes, the initial temperature is instead specified close to freezing temperature as $T_i = 0.01°\text{C}$ in the simulation.

The predicted ice thicknesses in Figure 10 show reasonably good agreement with experimental measurements from [6] even though there are slight differences in initial and boundary conditions. For the temperature history shown in Figure 11, nodal temperatures still exhibit step-like characteristics as in case 1 (Figure 4). The temperature at boundary, calculated from the (9), increases as the first cell undergone freezing due to the increasing value of k^f as more water in the first control volume turns to ice and, hence, the denominator $h + (k^f/d^f)$. Since the heat flux leaving the system is a function of temperature difference between the boundary and environment, as described in (3), the boundary flux or cooling rate in Figure 12 displays a similar profile.

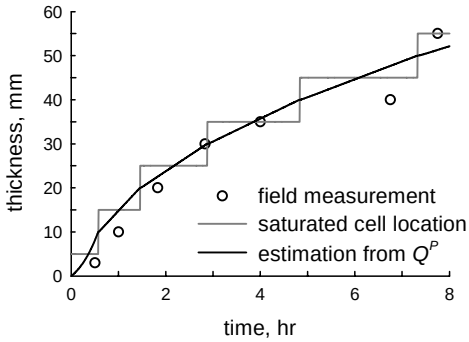

Figure 10 Case 2: Comparison of ice thickness for 1D convective problem. The field data is obtained with slightly different conditions and additional 3.7 mm-thick stainless steel mould [6].

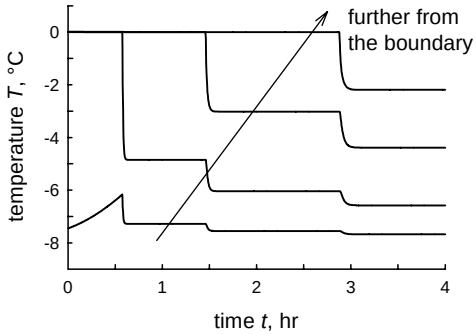

Figure 11 Case 2: Temperature at the boundary and 3 adjacent nodes.

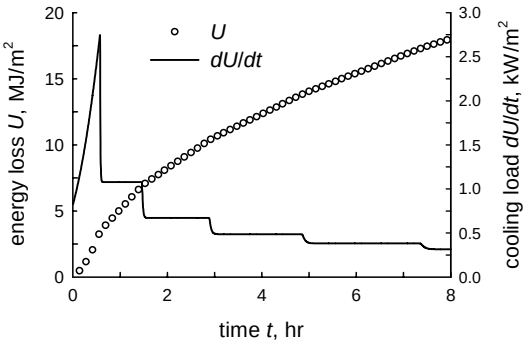

Figure 12 Case 2: Loss of internal energy and the cooling loads of the system.

4.3 Case 3: 3D Case Study

The developed program is employed to study the freezing process in industrial ice block manufacturing with a typical size of ice block shown in Figure 13a. Initially, temperature of water is $T_i = 30\ °\text{C}$ throughout. The boundary conditions on the top end is assumed to be $T_b = -1°\text{C}$ and $T_b = -10°\text{C}$ for the rest.

Due to symmetry, only one-fourth of the total area is modelled. The simulation uses the explicit/k_S schemes and mechanical properties of case 1. The grid consists of 28 × 13 × 140 cells while $\delta t = 10$ s.

Selected locations in the ice block are monitored (Figure 13b) and the temperatures and ice fractions at these nodes are shown in Figure 14 and Figure 15, respectively. For overall

results, the loss of internal energy and fraction of ice in the block is displayed in Figure 16.

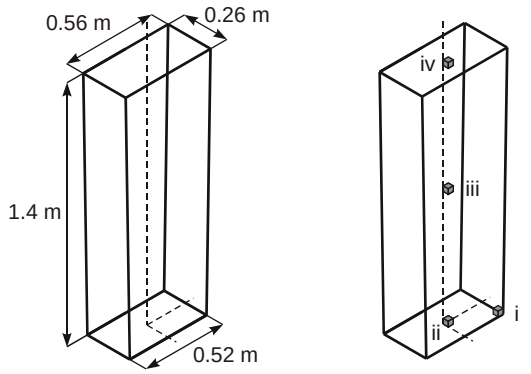

a) block geometry b) monitored cells

Figure 13 Case 3: Geometry and domain of ice block.

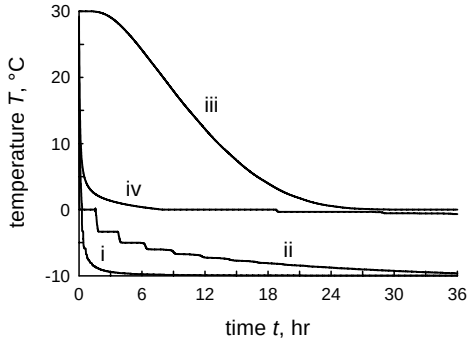

Figure 14 Case 3: Temperature history at monitoring locations.

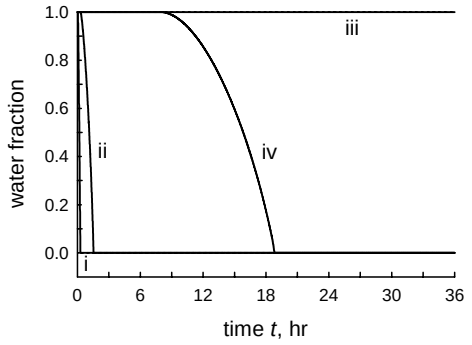

Figure 15 Case 3: Ice fraction at monitoring locations.

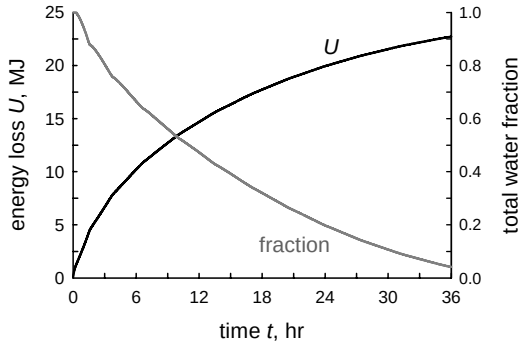

Figure 16 Case 3: Loss of internal energy and ice fraction for the one-quarter block system.

5. Conclusions

The ice formation modelling by the unstructured finite volume method with the fixed grid and the latent heat by fictitious sensible heat schemes is successfully performed. Two temporal schemes are compared – the explicit and pseudo-implicit – while the uses of continuously changing normal and harmonic mean conductivities are considered in addition to the solid value. The convection boundary is also studied.

Unlike [1], the emphasis of this works is on the actual applications, hence the main parameters of interest are those that can be directly applied to the efficiency improvement – the heat flux, fraction of water/ice and rate of ice formation. The heat flux leaving the ice block represents the cooling rate or the energy that is needed to be removed so that the water is cooled down and frozen. The fraction of water/ice and the rate of ice formation in the lesser degree are used to predict the time that the ice can be sold, and, thus, minimise the use of energy while ensuring the just-in-time availability of ice stock. Form the first case, the use of explicit and solid conductivity is recommended due to the superior prediction of ice thickness, hence, the rate of ice formation.

Even though the present 3D program is found to be sufficient accurate for the current project for an ice manufacturer in Samut Sakhon with saving of more than 2 Baht per block in the first month [5], it should be further developed and refined to ensure that it can model complex conditions, particularly, the fluctuations of main parameters in the real working conditions as well as the ease of use on site so that the plane performances can be easily optimised. Immediate future developments will be focus on the addition of heat convection, ice expansions and data mining.

6. Acknowledgement

Special thanks are due to Dr. Naebboon Hoonchareon and Miss Thitima Lertpiya, who are the true driving forces behind this work, as well as Dr. Chittin Tangthieng for providing field data. The tensor library was developed with the support from the Automation System for Advanced Manufacturing Project, a State and Industrial Cooperation on Research Project.

References

1. Prapainop, R. and Maneeratana, K. “Simulation of ice formation by the finite volume method”, Songklanakarin J. Sci. Technol., vol. 26, no. 1, pp. 55-70, 2004.
2. Wattananukulchai, W. and Maneeratana, K. “Local grid refinement by residual error estimation for heat conduction simulation with finite volume method”, Proceedings of ME-NETT 18, Khon Kaen, 18-20 October 2004.
3. Patankar, S. “Numerical Heat Transfer and Fluid Flow”, Hemisphere, New York, 1980.
4. Ozisik, M. N. “Heat Conduction”, 2nd ed., Wiley, 1993.
5. Hoonchareon, N. “Private Communication”, 2005.
6. Piruchvet, N. and Tangthieng, C. “A numerical study to predict the ice thickness, the ice production rate and the cooling load of the block-ice making process”, Proceedings of ME-NETT 18, Khon Kaen, 18-20 October 2004.